

1 **The Normalized Difference Infrared Index (NDII) as a proxy for root** 2 **zone moisture storage capacity**

3

4 N. Sriwongsitanon¹, H. Gao², H. H. G. Savenije², E. Maekan¹, S. Saengsawang¹, S. Thianpopirug¹

5 [1]{Department of Water Resources Engineering, Faculty of Engineering, Kasetsart University}

6 [2]{Water Resources Section, Delft University of Technology, Delft, the Netherlands}

7 Correspondence to: N. Sriwongsitanon (fengnns@ku.ac.th)

8

9 **Abstract**

10 With remote sensing we can readily observe the Earth's surface, but looking under the surface into
11 the root zone of vegetation is still a challenge. Yet knowledge on the dynamics of soil moisture in
12 the root zone is essential for agriculture, land-atmosphere interaction and hydrological modelling,
13 alike. In this paper we developed a novel approach to estimate the soil moisture storage deficit in
14 the root zone of vegetation, by using the remotely sensed Normalised Difference Infrared Index
15 (NDII) in the Upper Ping River Basin (UPRB) in Northern Thailand. Satellite data from the
16 Moderate Resolution Imaging Spectro-radiometer (MODIS) was used to evaluate the NDII over
17 an 8-day period, covering the study area from 2001 to 2013. The results show that NDII values
18 decrease sharply at the end of the wet season in October and reach lowest values near the end of
19 the dry season in March. The values then increase abruptly after rains have started, but vary in an
20 insignificant manner from the middle to the late rainy season. The NDII proves to be a very strong
21 proxy for moisture storage deficit in the root zone, which is a crucial component of hydrological
22 models. In addition, the NDII appears to be a reliable indicator for the temporal and spatial
23 distribution of drought conditions in the UPRB. During periods of moisture stress, the 8-day
24 average NDII values were found to correlate very well with the 8-day average soil moisture
25 content (S_u) simulated by the lumped conceptual hydrological rainfall-runoff model FLEX^L for 8
26 sub-catchments in the Upper Ping basin. Even the deseasonalized S_u and NDII (after subtracting
27 the dominant seasonal signal) showed good correlation during periods of moisture stress. The
28 results clearly demonstrate the feasibility of NDII as a proxy for root zone moisture stress. In dry
29 periods, when plants are exposed to water stress, the leaf-water deficit increases steadily, and
30 moisture stress in the leaves is connected to moisture deficits in the root zone. Once leaf-water is
31 close to saturation - mostly during the heart of the wet season - leaf characteristics and NDII
32 values are not well correlated. However, to constrain hydrological models or for water

33 management the stress periods are most important, which is why this product can be practical for
34 both hydrological modelling and water management.

35

36 **1. Introduction**

37 Estimating the moisture content of the soil from remote sensing is one of the main challenges in
38 the field of hydrology (e.g. [De Jeu et al., 2008](#); [Entekhabi et al., 2010](#)). Soil moisture is generally
39 seen as the key hydrological state variable determining the partitioning of fluxes (into direct
40 runoff, recharge and evaporation) ([Liang et. al., 1994](#)), the interaction with the atmosphere
41 ([Legates et. al., 2011](#)), and the carbon cycle ([Porporato et al., 2004](#)). The root zone of ecosystems,
42 being the dynamic part of the unsaturated zone, is the key part of the soil related to numerous sub-
43 surface processes ([Shukla and Mintz, 1982](#)). Several remote sensing products have been developed
44 especially for monitoring soil moisture (e.g. SMOS, ERS and AMSR-E), but until now
45 correlations between remote sensing products and observed soil moisture at different depths have
46 been modest at best ([Parajka et al., 2006](#); [Ford et al., 1997](#)). There are a few possible explanations.
47 One is that it is not (yet) possible to look into the soil deep enough to observe soil moisture in the
48 root zone of vegetation ([Shi et al., 1997](#); [Entekhabi et al., 2010](#)), second is that soil moisture
49 observations at certain depths are maybe not the right indicators for the moisture storage in the
50 root zone ([Mahmood and Hubbard, 2007](#)).

51 The hypothesis is that we can derive the soil moisture storage in the root zone from observing the
52 moisture state of the vegetation. We hypothesize that we can link the root zone moisture storage to
53 the water content of the leaves, because soil moisture suction pressure and moisture content in the
54 leaves are directly connected. Water is one of the determinant environmental variables for
55 vegetation growth, especially in water-limited ecosystems during dry periods. From plant
56 physiology point of view, water absorption from the root zone is driven by osmosis. Subsequently,
57 water transport from the roots to the leaves is driven by water potential differences, caused by
58 diffusion of water out of stomata, which we call transpiration. This physiological relationship
59 supports the correlation between root zone soil moisture, moisture tension in the leaves and the
60 water content of plants. In this paper we try to relate a remote sensing product (the NDII,
61 Normalised Difference Infrared Index) to the root zone storage of a conceptual hydrological
62 model, being a key state variable in the short and long term dynamics of the rainfall-runoff signal.
63 In order to do so, we calibrated a conceptual rainfall-runoff model to observed time series in sub-
64 basins of the Upper Ping river basin in Thailand and subsequently compared the temporal
65 variability of the root zone storage to the NDII.

66 The NDII was developed by [Hunt and Rock \(1989\)](#) using ratios of different values of near infrared
67 reflectance (NIR) and short wave infrared reflectance (SWIR), defined by:
68 $(\rho_{\text{NIR}} - \rho_{\text{SWIR}}) / (\rho_{\text{NIR}} + \rho_{\text{SWIR}})$, similar to the NDVI, which is defined by discrete red and near infrared.
69 NDII can be effectively used to detect plant water stress according to the property of shortwave
70 infrared reflectance, which is negatively related to leaf water content due to the large absorption
71 by the leaf (e.g. [Steele-Dunne et al., 2012](#); [Friesen et al., 2012](#); [Van Emmerik et al., 2015](#)). Many
72 studies have found relationships between the equivalent water thickness (EWT) and reflectance at
73 the near-infrared (NIR) and shortwave infrared (SWIR) portion of the spectrum used for deriving
74 NDII ([Hunt and Rock, 1989](#); [Gao, 1996](#); [Ceccato et al., 2002](#); [Fensholt and Sandholt, 2003](#)).
75 [Yilmaz et al. \(2008\)](#) found a significant linear relationship ($R^2 = 0.85$) between equivalent water
76 thickness (EWT) and NDII. They also discovered a significant relationship between vegetation
77 water content (VWC), the most successful parameter for retrieval of soil moisture content from
78 microwave data, and EWT; and between EWT and NDII. VWC was therefore linearly related to
79 NDII. [Fensholt and Sandholt \(2003\)](#) derived a shortwave infrared water stress index (SIWSI or
80 NDII) on a daily basis and found a strong correlation with in situ top layer soil moisture
81 measurements from the semiarid Senegal in 2001 and 2002. NDII was therefore selected in this
82 study of the Upper Ping River Basin (UPRB) in northern Thailand because of its potential in
83 detecting equivalent water thickness within the leaves affected by soil moisture storage in the root
84 zone. The relationship between average NDII and root zone moisture storage was evaluated in
85 sub-basins of the UPRB to be used as an indicator to prove the effectiveness of NDII. However,
86 because the NDII is an indicator for water stress, the index is only expected to show a strong link
87 to moisture storage in the root zone when there is a soil moisture deficit. Without water stress
88 occurring within the leaves, particularly during wet periods, NDII would possibly not reflect
89 variation in root zone soil moisture content ([Korres et al., 2015](#)).

90 Instead of comparing the NDII to observed soil moisture by in-field instrumentation, here another
91 approach has been followed. To acquire the information on root zone soil moisture, the lumped
92 (basin average) FLEX^L conceptual hydrological rainfall-runoff model ([Fenicia et al., 2011](#); [Gao et
93 al., 2014a](#); [Gao et al., 2014b](#)) was used and calibrated on 8 runoff stations in sub-basins of the
94 UPRB. The simulated root zone storage variation was then compared to the sub-basin average
95 NDII values over the 8 sub-basins.

96 **2. Study site and data**

97 **2.1 Study site**

98 The Upper Ping River Basin (UPRB) is situated between latitude 17°14'30" to 19°47'52" N, and
99 longitude 98°4'30" to 99°22'30" E in Northern Thailand and can be separated into 14 sub-
100 basins (Fig. 1) (Mapiam, et al., 2014). It has an area of approximately 25,370 km² in the provinces
101 of Chiang Mai and Lam Phun. The basin landform ranges from an undulating to a rolling terrain
102 with steep hills at elevations of 1,500 to 2,000 m, and valleys of 330 to 500 m (Mapiam and
103 Sriwongsitanon, 2009; Sriwongsitanon, 2010). The Ping River originates in Chiang Dao district,
104 north of Chiang Mai, and flows downstream to the south to become the inflow for the Bhumiphol
105 dam - a large dam with an active storage capacity of about 9.7 billion m³ (Sriwongsitanon, 2010).
106 The climate of the region is controlled by tropical monsoons, with distinctive dry and wet seasons
107 and free from snow and ice. The rainy season is influenced by the southwest monsoon and brings
108 about mild to heavy rainfall between May and October. Annual average rainfall and runoff of the
109 UPRB are approximately 1,170 and 270 mm/y, respectively. Avoiding the influence of other
110 factors, these catchments are ideal cases to concentrate on the relationship between NDII and root
111 zone moisture storage (S_u). The land cover of the UPRB is dominated by forest (Sriwongsitanon
112 and Taesombat, 2011).

113 **2.2 Data Collection**

114 **2.2.1 Satellite data**

115 The satellite data used for calculating the NDII is the MODIS level 3 surface reflectance product
116 (MOD09A1), which is at 500 m resolution in an 8-day composite of the gridded level 2 surface
117 reflectance products. Each product pixel contains the best possible L2G observation during an 8-
118 day period as selected on the basis of high observation coverage, low view angle, absence of
119 clouds or cloud shadow, and aerosol loading. MOD09 (MODIS Surface Reflectance) is a seven-
120 band product, which provides an estimate of the surface spectral reflectance for each band as it
121 would have been measured at ground level without atmospheric scattering or absorption. This
122 product has been corrected for the effects of atmospheric gases and aerosols (Vermote et al.,
123 2011). The available MODIS data covering the UPRB from 2001 to 2013 were downloaded from
124 ftp://e4ftl01.cr.usgs.gov/MOLT. The HDF-EOS Conversion Tool was applied to extract the
125 desired bands (bands 2 (0.841-0.876 μ m) and 6 (1.628-1.652 μ m)) and re-projected into Universal
126 Transverse Mercator (Zone 47N, WGS84) from the original ISIN mapping grid.

127 **2.2.2 Rainfall data**

128 A total of 65 non-automatic rain-gauge stations were selected from 2001 to 2013. 42 stations are
129 located within the UPRB while 23 stations are situated in its surroundings. These rain gauges are
130 owned and operated by the Thai Meteorological Department and the Royal Irrigation Department.
131 Quality control of the rainfall data was performed by comparing them to adjacent rainfall data.
132 Rainfall is used as the forcing data of the hydrological model.

133 **2.2.3 Runoff data**

134 Daily runoff data from 1995 to 2011 at 8 stations located in the UPRB were adequate to be used
135 for FLEX^L calibration. These 8 stations are operated by the Royal Irrigation Department in
136 Thailand. The locations of these 8 stations and the associated sub-basins are shown in Fig. 1.
137 Runoff data at these stations are not affected by large reservoirs and have been checked for their
138 reliability by comparing them with rainfall data covering their catchment areas at the same
139 periods. Catchment characteristics and available data periods for model calibration of the selected
140 8 sub-basins are summarized in Table 3.

141 **2.3 NDII drought index for the UPRB**

142 The NDII from 2001 to 2013, covering the UPRB, was computed using MODIS bands 2 and 6
143 reflectance data. The 8-day surface reflectance data of near infrared (band 2: wavelength between
144 0.841-0.876 μm) and short wave infrared (band 6: wavelength between 1.628-1.652 μm) are
145 described by Eq. (1). The 8-day NDII values were averaged over each sub-basin to allow
146 comparison to the 8-day average S_u (root zone storage reservoir) values extracted from the FLEX^L
147 model results at each of the 8 runoff stations.

148

149 **3. Methods**

150 **3.1 Estimating vegetation water content using near infrared and short wave infrared**

151 Estimates of vegetation water content (the amount of water in stems and leaves) are of interest to
152 assess the vegetation water status in agriculture and forestry and have been used for drought
153 assessment (Cheng et al., 2006; Gao, 1996; Gao and Goetz, 1995; Ustin et al., 2004; Peñuelas et
154 al., 1993). Evidence of physically-based radiative transfer models and laboratory studies have
155 proved that changes in water content in plant tissues have a large effect on the leaf reflectance in
156 several regions of the 0.7-2.5 μm spectrum (Fensholt and Sandholt, 2003). Tucker (1980)
157 suggested that the spectral interval between 1.55 and 1.75 μm (SWIR) is the most suitable region

158 for remotely sensed leaf water content. It is well known that these wavelengths are negatively
159 related to leaf water content due to a large absorption by leaf water (Tucker, 1980; Ceccato et al.,
160 2002). However, variations in leaf internal structure and leaf dry matter content also influence the
161 SWIR reflectance. Therefore, only SWIR reflectance values are not suitable for retrieving
162 vegetation water content. To improve the accuracy in retrieving the vegetation water content, a
163 combination of SWIR and NIR (0.7 to 0.9 μm) reflectance information was utilized because NIR
164 is only affected by leaf internal structure and leaf dry matter content but not by water content. A
165 combination of SWIR and NIR reflectance information can remove the effect of leaf internal
166 structure and leaf dry matter content and can improve the accuracy in retrieving the vegetation
167 water content (Ceccato et al., 2001; Yilmaz et al., 2008; Fensholt and Sandholt, 2003).

168 On the basis of this idea, Fensholt and Sandholt (2003) derived NDII:

$$169 \quad NDII = \frac{\rho_{0.85} - \rho_{1.65}}{\rho_{0.85} + \rho_{1.65}} \quad (1)$$

170 where $\rho_{0.85}$ and $\rho_{1.65}$ are the reflectances at 0.85 μm and 1.65 μm wavelengths, respectively. NDII
171 is a normalized index and the values theoretically vary between -1 and 1. A low NDII value and
172 especially below zero means that reflectance from $\rho_{0.85}$ is lower than the reflectance from $\rho_{1.65}$
173 which indicates canopy water stress.

174 **3.2 FLEX^L Model**

175 FLEX^L (Fig. 2) is a lumped conceptual hydrological model which has an HBV-like model
176 structure developed in a flexible modelling framework (Fenicia et al., 2011; Gao et al., 2014a; Gao
177 et al., 2014b). The model structure comprises four conceptual reservoirs: the interception reservoir
178 S_i (mm), the unsaturated reservoir representing the moisture storage in the root zone S_u (mm), the
179 fast response reservoir S_f (mm), and the slow response reservoir S_s (mm). It also includes two lag
180 functions representing the lag time from storm to peak flow (T_{lagF}), and the lag time of recharge
181 from the root zone to the groundwater (T_{lagS}). Besides a water balance equation, each reservoir has
182 process equations that connect the fluxes entering or leaving the storage compartment to the
183 storage in the reservoirs (so-called constitutive functions). Table 1 shows 15 mathematical
184 expressions used for modelling the FLEX^L. A total of 11 model parameters with their distribution
185 values are shown in Table 2 and they have to be identified by model calibration. Forcing data
186 include the elevation-corrected daily average rainfall (Gao et al., 2014a), daily average, minimum
187 and maximum air temperature, and potential evaporation derived by Hargreaves equation
188 (Hargreaves and Samani, 1985).

189 3.2.1 Interception reservoir

190 The interception evaporation E_i (mm d^{-1}) is calculated by potential evaporation E_0 (mm d^{-1}) and
191 the storage of the interception reservoir S_i (mm) (Eq. (3)). There is no effective rainfall P_e (mm d^{-1})
192 as long as the S_i is less than its storage capacity $S_{i,\max}$ (mm) (Eq. (4)) (de Groen and Savenije,
193 2006).

194 3.2.2 Unsaturated root zone reservoir

195 The unsaturated root zone reservoir partitions effective rainfall into infiltration, and runoff R (mm
196 d^{-1}), and determines the transpiration by vegetation. Therefore, it is the core of the FLEX^L model.
197 In this study, we applied the widely used beta function (Eq. (6)) of the Xinanjiang model (Zhao,
198 1992; Liang et al., 1992), developed based on the variable contribution area theory (Hewlett and
199 Hibbert, 1967; Beven, 1979), but which can equally reflect the spatial probability distribution of
200 runoff thresholds. The beta function defines the runoff percentage C_r (-) for each time step as a
201 function of the relative soil moisture content ($S_u/S_{u,\max}$). In Eq. (6), $S_{u,\max}$ (mm) is the root zone
202 storage capacity, and β (-) is the shape parameter describing the spatial distribution of the root
203 zone storage capacity over the catchment. In Eq. (7), the relative soil moisture and potential
204 evaporation are used to determine the transpiration E_t (mm d^{-1}); C_e (-) indicates the fraction of
205 $S_{u,\max}$ above which the transpiration is no longer limited by soil moisture stress ($E_t = E_0 - E_i$).

206 3.2.3 Response routine

207 In Eq. (8), R_f (mm d^{-1}) indicates the flow into the fast response routine; D (-) is a splitter to
208 separate recharge from preferential flow. In Eq. (9), R_s (mm d^{-1}) indicates the flow into the
209 groundwater reservoir. Equation (10) and (11) are used to describe the lag time between storm and
210 peak flow. $R_f(t-i+1)$ is the generated fast runoff from the unsaturated zone at time $t-i+1$; T_{lag} is a
211 parameter which represents the time lag between storm and fast runoff generation; $c(i)$ is the
212 weight of the flow in $i-1$ days before; and $R_{\text{fl}}(t)$ is the discharge into the fast response reservoir
213 after convolution.

214 The linear response reservoirs, representing linear relationships between storages and releases, are
215 applied to conceptualize the discharge from the surface runoff reservoir, fast response reservoir
216 and slow response reservoir. In Eq. (12), Q_{ff} (mm d^{-1}) is the surface runoff, with timescale K_{ff} (d),
217 activated when the storage of fast response reservoir exceeds the threshold $S_{\text{f,max}}$ (mm). In Eq. (14)
218 and (16), Q_f (mm d^{-1}) and Q_s (mm d^{-1}) represent the fast and slow runoff; K_f (d) and K_s (d) are the

219 time scales of the fast and slow runoff, respectively. Q_m (mm d^{-1}) is the total amount of runoff
220 simulated from the three individual components, including Q_{ff} , Q_f , and Q_s .

221 **3.2.4 Model calibration**

222 A multi-objective calibration strategy has been adopted in this study to allow for the model to
223 effectively reproduce different aspects of the hydrological response, i.e. high flow, low flow and
224 the flow duration curve. The model was therefore calibrated to three Kling-Gupta efficiencies
225 (Gupta et al., 2009): 1) the K-G efficiency of flows (I_{KGE}) measures the performance of
226 hydrograph reproduction especially for high flows; 2) the K-G efficiency of the logarithm of flows
227 emphasizes low flows (I_{KGL}), and 3) the K-G efficiency of the flow duration curve (I_{KGF}) to
228 represent the flow statistics.

229 The MOSCEM-UA (Multi-Objective Shuffled Complex Evolution Metropolis-University of
230 Arizona) algorithm (Vrugt et al., 2003) was used as the calibration algorithm to find the Pareto-
231 optimal solutions defined by the mentioned three objective functions. This algorithm requires 3
232 parameters including the maximum number of iterations, the number of complexes, and the
233 number of random samples that is used to initialize each complex. To ensure fair comparison, the
234 parameters of MOSCEM-UA were set based on the number of model parameters. Therefore, the
235 number of complexes is equal to the number of free parameters n ; the number of random samples
236 is equal to $n*n*10$; and the number of iterations was set to 30000. The model is a widely validated
237 model, which is only used here to derive the magnitude of the root zone moisture storage.
238 Therefore validation is not considered necessary, since the model is merely meant to compare
239 calibrated values of S_u with NDII.

240 **3.3 Deseasonalization**

241 Seasonal signals exist both in NDII and S_u time series. This can lead to spurious correlation.
242 Therefore we deseasonalized both signals to eliminate this strong signal (Schaeffli & Gupta, 2007)
243 and subsequently compare the deviations from the seasonal signals of both NDII and S_u . Firstly,
244 the NDII and S_u were normalized between 0 and 1. Then seasonal patterns of NDII and S_u were
245 determined as the average seasonal signals, after which these were subtracted from the normalised
246 data.

247

248 **4. Results**

249 **4.1 Spatial and seasonal variation of NDII values for the UPRB and its 14 sub-basins**

250 To demonstrate the spatial and seasonal behaviour of the NDII over the UPRB, the 8-day NDII
251 values were aggregated to monthly values for 2001 to 2013. Figure 3 shows examples of monthly
252 average NDII values for the UPRB in 2004, which is the year with the lowest annual average NDII
253 value. The figure shows that NDII values are higher during the wet season (May to October) and
254 lower during the dry season (from November to April). The lower amounts of rainfall between
255 November and April cause a continuous reduction of NDII values. On the other hand, higher
256 amounts of rainfall between May and October result in increasing NDII values. However, NDII
257 values appear to vary little between July and October.

258 The average NDII values during the wet season, the dry season, and the whole year within the 13
259 years are presented in Table 4. The table also shows the order of the NDII values from the highest
260 (number 1) to the lowest (number 13). It can be seen that the annual average NDII value for the
261 whole basin is approximately 0.165, while the average values during the wet and dry season are
262 about 0.211 and 0.118, respectively. The highest mean annual value (NDII = 0.177) occurred in
263 2002-2003 and the lowest (NDII = 0.149) in 2004-2005. The highest (NDII = 0.149) and lowest
264 (NDII = 0.088) dry season values were reported in 2002-2003 and 2004-2005, respectively. On the
265 other hand, the highest (NDII = 0.224) and lowest (NDII = 0.197) wet season values were
266 observed in 2006-2007 and 2010-2011, respectively. It can be concluded that a dry season with
267 relatively low moisture content and a wet season with high moisture content as specified by NDII
268 values do not normally occur in the same year.

269 The 8-day NDII values were also computed for each of the 14 tributaries within the UPRB from
270 2001 to 2013. Table 5 shows the monthly averaged NDII values between 2001 and 2013 and the
271 ranking order for each of the 14 tributaries. The results suggest that Nam Mae Taeng, Nam Mae
272 Rim, and Upper Mae Chaem sub-basins, which have higher mean annual NDII values, have a
273 higher moisture content than other sub-basins; while Nam Mae Haad, Nam Mae Li, and Ping
274 River Section 2 are 3 sub-basins, with lower mean annual NDII values, have lower moisture
275 content than other sub-basins. Monthly average NDII values for these 6 sub-basins are presented
276 in Fig. 4. It can be seen that during the dry season, NDII values of the 3 sub-basins with the lowest
277 values are a lot lower than those of the 3 sub-basins with the highest NDII values. However, NDII
278 values for these 2 groups are not significantly different during the wet season. The figure also
279 reveals that NDII values tend to continuously increase from relatively low values in March to
280 higher values in June. The values slightly fluctuate during the wet season before sharply falling
281 once again when the rainy season ends, and reach their minimum values in February.

282 **4.2 FLEX^L Model results**

283 Calibration of FLEX^L was done on the 8 sub-catchments which have runoff stations. The results
284 are summarized in Table 6. The performance of the model was quite good as demonstrated in
285 Table 7. In Fig. 5, the duration curves of runoff stations P.20 and P.21 are presented as examples
286 of model performance. Table 7 shows the average Kling-Gupta efficiencies values for I_{KGE} , I_{KGL}
287 and I_{KGF} , which indicate the performance of high flows, low flows, and flow duration curve for the
288 8 runoff stations. The results for the flow duration curve appear to be better than those of the high
289 flows and especially the low flows. However, the overall results are acceptable and can be used for
290 further analysis in this study.

291 **4.3 Relation between NDII and root zone moisture storage (S_u)**

292 The 8-day NDII values were compared to the 8 day average root zone moisture storage values of
293 the FLEX^L model. It appears that during moisture stress periods, the relationship can be well
294 described by an exponential function, for each of the 8 sub-catchments. Table 8 presents the
295 coefficients of the exponential relationships as well as the coefficients of determination (R^2) for
296 annual, wet season, and dry season values for each sub-catchment. The corresponding scatter plots
297 are shown in Fig. 6. It can be clearly seen that the correlation is much better in the dry season than
298 in the wet season. During the wet season, there may also be short period of moisture stress, where
299 the exponential pattern can be recognized, but no clear relation is found when the vegetation does
300 not experience any moisture stress.

301 Examples of scaled time series of NDII and root zone storage (S_u) values for the sub-catchments
302 P.20 and P.21 are presented in Figure 7, respectively. The scaled time series of the NDII and S_u
303 values were calculated by dividing their value by the differences between their maximum and
304 minimum values: $NDII/(NDII_{max}-NDII_{min})$ and $S_u/(S_{u,max}-S_{u,min})$, respectively, while the maximum
305 and the minimum are the values within the overall considered time series. Figure 7 shows that the
306 scaled NDII and S_u values are highly correlated during the dry season, but less so during the wet
307 season. These results confirm the potential of NDII to effectively reflect the vegetation water
308 content, which, through the suction pressure exercised by the moisture deficit, relates to the
309 moisture content in the root zone. During dry periods, or during dry spells in the rainy season, as
310 soon as the leaves of the vegetation experience suction pressure, we see high values of the
311 coefficient of determination.

312 If the soil moisture in the root zone is above a certain threshold value, then the leaves are not
313 under stress. In the UPRB this situation occurs typically during the middle and late rainy season.
314 The NDII then does not vary significantly while the root zone moisture storage may still vary,
315 albeit above the threshold where moisture stress occurs. This causes a lower correlation between

316 NDII and root zone storage during wet periods. Interestingly, even during the wet season dry
317 spells can occur. We can see in Fig. 6, that during such a dry spell, the NDII and S_u again follow
318 the exponential relationship.

319

320 We can see that the S_u , derived merely from precipitation and energy, is strongly correlated to the
321 vegetation water observed by NDII during condition of moisture stress, without time lag (Figure 6,
322 S1, S2). Introduction of a time lag resulted in reduction of the correlation coefficients
323 (Supplementary material). This confirms the direct response of vegetation to soil moisture stress,
324 which confirms that the NDII can be used as a proxy for root zone moisture storage.

325 The deseasonalized results of dry periods in sub-catchments P.20 and P.21 are shown in Figure 7.
326 We found these variations of deseasonalized NDII and S_u to be similar in these two sub-
327 catchments, with the coefficients of determination (R^2) as 0.32 and 0.18 respectively in P.20 and
328 P.21. More important than the coefficient of determination is the similarity between the
329 deseasonalized patterns. For P.20, the year 2001 is almost identical, whereas the years 2004 and
330 2006 are dissimilar. In general the patterns are well reproduced, especially if we take into account
331 the implicit uncertainties of the lumped hydrological model and the data of precipitation and
332 potential evaporation used in the model. The results of other sub-basins can be found in the
333 supplementary materials.

334

335 **5. Discussion**

336 **5.1 Is vegetation a trouble-maker or a good indicator for moisture storage in the root zone?**

337 In bare soil, remote sensors can only detect soil moisture until a few centimeters below the surface
338 (~5cm) (Entekhabi et al., 2010). Unfortunately, for hydrological modelling, the moisture state of
339 the bare surface is of only limited interest. What is of key interest for understanding the dynamics
340 of hydrological systems is the variability of the moisture storage in the unsaturated zone. This
341 variability determines the rainfall-runoff behaviour, the transpiration of vegetation, and the
342 partitioning between different hydrological fluxes. This dynamic part of the unsaturated zone is
343 the root zone of ecosystems. However, observing the soil moisture content in the root zone is still
344 a major challenge (Entekhabi et al., 2010).

345 What is normally done, is to link the moisture content of the surface layer to the total amount of
346 moisture in the root zone. Knowing the surface soil moisture, the root zone soil moisture can be

347 estimated by an exponential decay filter (Albergel et al., 2008; Ford et al., 2014) or by models
348 (Reichle, 2008). However, the surface soil moisture is only weakly related with root zone soil
349 moisture (Mahmood and Hubbard, 2007); it only works if there is connectivity between the
350 surface and deeper layers and when a certain state of equilibrium has been reached (when the short
351 term dynamics after a rainfall event has leveled out). It is also observed that the presence of
352 vegetation prevents the observation of soil moisture and further deteriorates the results (Jackson
353 and Schmugge, 1991). Avoiding the influence of vegetation in observing soil moisture (e.g. by
354 SMOS or SMAP) is seen as a challenge by some in the remote sensing community (Kerr et al.,
355 2001; Entekhabi et al., 2010). Several algorithms have been proposed to filter out the vegetation
356 impact (Jackson and Schmugge, 1991). But is vegetation a trouble-maker, or does it offer an
357 excellent opportunity to directly gauge the state of the soil moisture?

358 In this study, we found that vegetation rather than a problem could become key to sensing the
359 storage of moisture in the root zone. The water content in the leaves is connected to the suction
360 pressure in the root zone (Rutter and Sands, 1958). If the suction pressure is above a certain
361 threshold, then this connection is direct and very sensitive. We found a highly significant
362 correlation between NDII and S_u , particularly during periods of moisture stress. During dry
363 periods, or during dry spells in the rainy season, as soon as the leaves of the vegetation experience
364 suction pressure, we see high values of the coefficient of determination. Observing the moisture
365 content of vegetation provides us with directly information on the soil moisture state in the root
366 zone. We also found that there is almost no lag time between S_u and NDII. This illustrates the fast
367 response of vegetation to soil moisture variation, which makes the NDII a sensitive and direct
368 indicator for root zone moisture storage.

369 **5.2 Implication in hydrological modelling**

370 Simulation of root zone soil moisture is crucial in hydrological modelling (Houser et al., 1998;
371 Western and Blöschl, 1999). Using estimates of soil moisture states could increase model
372 performance and realism, but moreover, it would be powerful information to facilitate prediction
373 in ungauged basins (Hrachowitz et al., 2013). However, until now, it has not been practical (e.g.
374 Parajka et al., 2006; Entekhabi et al., 2010). Assimilating soil moisture in hydrological models,
375 either from top-soil observation by remote sensing, or from the deeper soil column by models
376 (Reichle, 2008), is still a challenge. Several studies showed how difficult it is to assimilate soil
377 moisture data to improve daily runoff simulation (Parajka et al., 2006; Matgen et al., 2012).

378 There are several reasons why we have not compared our results with soil moisture observations in
379 the field. Firstly, observations of soil moisture are not widely available. Moreover, it is not

380 straightforward to link classical soil moisture observations to the actual moisture available in the
381 root zone. Most observations are conducted at fixed depths and at certain locations within a highly
382 heterogeneous environment. Without knowing the details of the root distribution both in the
383 horizontal and vertical plain, it is hard, if not impossible, to estimate root zone soil moisture. We
384 should realize that it is difficult to observe root zone soil moisture even at a local scale. But
385 measuring root zone soil moisture at a catchment scale is even more challenging. State-of-the-art
386 remote sensing techniques can observe spatially distributed soil moisture, but what they can see is
387 only the top layer if not blocked by vegetation. The top layer moisture may be correlated with the
388 root zone storage, but it is definitely not the same.

389 By observing the moisture content of the leaves, the NDII represents the soil moisture storage
390 condition of the entire root zone, which is precisely the information that hydrological models
391 require. This study clearly shows the strong temporal correlation between S_u and NDII. From the
392 relationship between NDII and S_u , we can directly derive a proxy for the soil moisture state, which
393 can potentially be assimilated in hydrological models. This method would be extremely useful for
394 prediction of discharge in ungauged basins.

395 We should, of course, be aware of regional limitations. This study considered a tropical seasonal
396 evergreen ecosystem, where periods of moisture stress regularly occur. In ecosystems which shed
397 their leaves, or go dormant, other conditions may apply. We need further investigations into the
398 usefulness of this approach in catchments with different climates. In addition, the phenology of the
399 ecosystem is of importance, which should be taken into consideration in follow-up research.

400

401 **6. Conclusions**

402 The NDII was used to investigate drought for the UPRB from 2001 to 2013. Monthly average
403 NDII values appear to be spatially distributed over the UPRB, in agreement with seasonal
404 variability and landscape characteristics. NDII values appear to be lower during the dry season and
405 higher during the wet season as a result of seasonal differences between precipitation and
406 evaporation. The NDII appears to correlate well with the moisture storage in the root zone,
407 offering an interesting proxy variable for calibration of hydrological models in ungauged basins.

408 To illustrate the importance of NDII as a proxy for root zone moisture storage in hydrological
409 models, we applied the FLEX^L model to assess the root zone soil moisture content (S_u) of 8 sub-
410 catchments of the UPRB controlled by 8 runoff stations. The results show that the 8-day average
411 NDII values over the study sub-basin correlate well with the 8-day average S_u for all sub-
412 catchments during dry periods (average R^2 equals 0.87), and less so during wet spells (average R^2

413 equals 0.61). The NDII appears to be a good proxy for root zone moisture content during dry
414 spells when leaves are under moisture stress. The natural interaction between rainfall, soil
415 moisture, and leaf water content can be visualised by the NDII, making it an important indicator
416 both for hydrological modelling and drought assessment.

417

418 **Acknowledgement**

419 We gratefully acknowledge Kasetsart University Research and Development Institute for
420 financially supporting this research. We also appreciate Royal Irrigation Department and Thai
421 Meteorological Department for providing the rainfall data. Finally, we sincerely thank the MODIS
422 Land Discipline Group for creating and sharing the MODIS LAND data used in this study.

423

424 **References**

425 Albergel, C., Rüdiger, C., Pellarin, T., Calvet, J. C., Fritz, N., Froissard, F., Suquia, D., Petitpa, A.,
426 Piguet, B., and Martin, E.: From near-surface to root-zone soil moisture using an exponential
427 filter: an assessment of the method based on in-situ observations and model simulations, *Hydrol.*
428 *Earth Syst. Sci.*, 12(6), 1323-1337, 2008.

429 Beven, K. J. and M. J. Kirkby. 1979. A physically based, variable contributing area model of basin
430 hydrology. *Hydrological Sciences Bulletin*. 24(1). 43-69.

431 Ceccato, P., Flasse, S., and Grégoire, J. M.: Designing a spectral index to estimate vegetation
432 water content from remote sensing data: Part 2, Validations and applications, *Remote Sens.*
433 *Environ.*, 82, 198–207, doi:10.1016/S0034-4257(02)00036-6, 2002.

434 Ceccato, P., Flasse, S., Tarantola, S., Jacquemoud, S., and Grégoire, J. M.: Detecting vegetation
435 leaf water content using reflectance in the optical domain, *Remote Sens. Environ.*, 77, 22– 33,
436 doi:10.1016/S0034-4257(01)00191-2, 2001.

437 Cheng, Y. B., Zarco-Tejada, P. J., Riaño, D., Rueda, C. A., and Ustin, S. L.: Estimating vegetation
438 water content with hyperspectral data for different canopy scenarios: Relationships between
439 AVIRIS and MODIS indexes, *Remote Sens. Environ.*, 105, 354–366,
440 doi:10.1016/j.rse.2006.07.005, 2006.

441 de Groen, M. M., and Savenije, H. H. G.: A monthly interception equation based on the statistical
442 characteristics of daily rainfall, *Water Resour. Res.*, 42, W12417, doi:10.1029/2006WR005013,
443 2006.

444 De Jeu, R. A. M., Wagner, W., Holmes, T. R. H., Dolman, A. J., van de Giesen, N. C., and
445 Friesen, J.: Global Soil Moisture Patterns Observed by Space Borne Microwave Radiometers and
446 Scatterometers, *Surv. Geophys.*, 28, 399–420, doi 10.1007/s10712-008-9044-0, 2008.

447 Entekhabi, D., Nioku, E. G., O'Neill, P. E., Kellogg, K. H., Crow, W. T., Edelstein, W. N., Entin,
448 J. K., Goodman, S. D., Jackson, T. J., Johnson, J., Kimball, J., Piepmeier, J. R., Koster, R. D.,
449 Martin, N., McDonald, K. C., Moghaddam, M., Moran, S., Reichle, R., Shi, J.-C., Spencer, M. W.,
450 Thurman, S. W., Leung, T., and Van Zyl, J.: The Soil Moisture Active Passive (SMAP) Mission,
451 *Proc. IEEE.*, 98, 704–716, 2010.

452 Fenicia, F., Kavetski, D., and Savenije, H. H. G.: Elements of a flexible approach for conceptual
453 hydrological modeling: 1. Motivation and theoretical development, *Water Resour. Res.*, 47,
454 W11510, doi:10.1029/2010WR010174, 2011.

455 Fensholt, R., and Sandholt, I.: Derivation of a shortwave infrared stress index from MODIS near-
456 and shortwave infrared data in a semiarid environment, *Remote Sens. Environ.*, 87, 111–121,
457 doi:10.1016/j.rse.2003.07.002, 2003.

458 Ford, T. W., Harris, E., and Quiring, S. M.: Estimating root zone soil moisture using near-surface
459 observations from SMOS, *Hydrol. Earth Syst. Sci.*, 18(1), 139-154, 2014.

460 Friesen, J., Steele-Dunne, S. C., and van de Giesen, N.: Diurnal Differences in Global ERS
461 Scatterometer Backscatter Observations of the Land Surface, *IEEE Transactions on Geoscience
462 and Remote Sensing*, vol. 50, issue 7, pp. 2595-2602, 2012.

463 Gao, B. C.: NDWI - A normalized difference water index for remote sensing of vegetation liquid
464 water from space, *Remote Sens. Environ.*, 58, 257–266, doi:10.1016/S0034-4257(96)00067-3,
465 1996.

466 Gao, B. C., and Goetz, A. F. H.: Retrieval of equivalent water thickness and information related to
467 biochemical components of vegetation canopies from AVIRIS data, *Remote Sens. Environ.*, 52,
468 155–162, doi:10.1016/0034-4257(95)00039-4, 1995.

469 Gao, H., Hrachowitz, M., Fenicia, F., Gharari, S., and Savenije, H. H. G.: Testing the realism of a
470 topography driven model (Flex-Topo) in the nested catchments of the Upper Heihe,
471 China, *Hydrol. Earth Syst. Sci.*, 18, 1895–1915, doi:10.5194/hess-18-1895-2014, 2014(a).

472 Gao, H., Hrachowitz, M., Schymanski, S. J., Fenicia, F., Sriwongsitanon, N., and Savenije, H. H.
473 G.: Climate controls how ecosystems size the root zone storage capacity at catchment scale,
474 *Geophys. Res. Lett.*, 41, 7916–7923, doi:10.1002/2014GL061668, 2014(b).

475 Gupta, H. V., Kling, H., Yilmaz, K. K., and Martinez, G. F.: Decomposition of the mean squared
476 error and NSE performance criteria: implications for improving hydrological modeling, *J. Hydrol.*,
477 377, 80–91, <http://dx.doi.org/10.1016/j.jhydrol.2009.08.003>, 2009.

478 Hargreaves GH, Samani ZA: Reference crop evapotranspiration from temperature. *Appl Engine*
479 *Agric.* 1(2):96–99, 1985.

480 Houser, P. R., Shuttleworth, W. J., Famiglietti, J. S., Gupta, H. V., Syed, K. H., and Goodrich, D.
481 C.: Integration of soil moisture remote sensing and hydrologic modeling using data assimilation,
482 edited, 1998.

483 Hunt, E. R. Jr. and Rock, B. N.: Detection of changes in leaf water content using near- and middle-
484 infrared reflectances, *Remote Sens. Environ.*, 30, 43–54, doi:10.1016/0034-4257(89)90046-1,
485 1989.

486 Hrachowitz, M., Savenije, H.H.G., Blöschl, G., McDonnell, J.J., Sivapalan, M., Pomeroy, J.W.,
487 Arheimer, B., Blume, T., Clark, M.P., Ehret, U., Fenicia, F., Freer, J.E., Gelfan, A., Gupta, H.V.,
488 Hughes, D.A., Hut, R.W., Montanari, A., Pande, S., Tetzlaff, D., Troch, P.A., Uhlenbrook, S.,
489 Wagener, T., Winsemius, H.C., Woods, R.A., Zehe, E., and Cudennec, C.: A decade of
490 Predictions in Ungauged Basins (PUB); a review. *Hydrol. Sci. J.*, 58 (6), 1–58, doi:
491 10.1080/02626667.2013.803183, 2013.

492 Hewlett, J.D. and Hibbert, A.R. 1967. Factors affecting the response of small watersheds to
493 precipitation in humid regions. IN *Forest Hydrology* (eds. W.E. Sopper and H.W. Lull). Pergamon
494 Press, Oxford. pp. 275-290.

495 Korres, W., Reichenau, T. G., Fiener, P., Koyama, C. N., Bogena, H. R., Cornelissen, T., Baatz,
496 R., Herbst, M., Diekkrüger, B., Vereecken, H., and Schneider, K.: Spatio-temporal soil moisture
497 patterns – A meta-analysis using plot to catchment scale data, *J. Hydrol.*, 520, 326–341,
498 [doi:10.1016/j.jhydrol.2014.11.042](http://dx.doi.org/10.1016/j.jhydrol.2014.11.042), 2015.

499 Jackson, T. J., and Schmugge, T. J.: Vegetation effects on the microwave emission of soils,
500 *Remote Sens. Environ.*, 36(3), 203-212, 1991.

501 Kerr, Y. H., Waldteufel, P., Wigneron, J.-P., Martinuzzi, J.-M., Font, J., and Berger, M.: Soil
502 Moisture Retrieval from Space: The Soil Moisture and Ocean Salinity (SMOS) Mission, *IEEE*
503 *Transactions on Geoscience and Remote Sensing*, 39(8), 1729-1735, 2001.

504 Legates, D. R., Mahmood, R., Levia, D. F., DeLiberty, T. L., Quiring, S. M., Houser, C., and
505 Nelson, F. E.: Soil moisture: A central and unifying theme in physical geography, *Prog. Phys.*
506 *Geogr.*, 35, 65–86, 2011.

507 Liang, X., Lettenmaier, D. P., Wood, E. F., and Burges, S. J.: A simple hydrologically based
508 model of land surface water and energy fluxes for general circulation models, *Journal of*
509 *Geophysical Research: Atmospheres*, 99, 14 415-14 428, 1994.

510 Mahmood, R., and Hubbard, K. G.: Relationship between soil moisture of near surface and
511 multiple depths of the root zone under heterogeneous land uses and varying hydroclimatic
512 conditions, *Hydrological Processes*, 25, 3449-3462, doi: 10.1002/hyp.6578, 2004.

513 Mapiam, P. P., Sharma, A., and Sriwongsitanon, N.: Defining the Z~R relationship using gauge
514 rainfall with coarse temporal resolution: Implications for flood forecast. *J. Hydrol. Eng.*, 19,
515 04014004, doi: 10.1061/(ASCE)HE.1943-5584.0000616, 2014.

516 Mapiam, P. P., and Sriwongsitanon, N.: Estimation of the URBS model parameters for flood
517 estimation of ungauged catchments in the upper Ping river basin, Thailand. *ScienceAsia*, 35, 49–
518 56, 2009.

519 Matgen P, Fenicia F, Heitz S, Plaza D, de Keyser R, Pauwels VRN, et al. Can ASCAT-derived
520 soil wetness indices reduce predictive uncertainty in well-gauged areas? A comparison with in situ
521 observed soil moisture in an assimilation application. *Adv Water Resour* 2012;44:49–65.
522 doi:http://dx.doi.org/10.1016/j.advwatres.2012.03.022.

523 Parajka, J., Naeimi, V., Blöschl, G., Wagner, W., Merz, R., and Scipal, K.: Assimilating
524 scatterometer soil moisture data into conceptual hydrologic models at the regional scale, *Hydrol.*
525 *Earth Syst. Sci.*, 10(3), 353-368, 2006.

526 Peñuelas, J., Filella, I., Biel, C., Serrano, L., and Savé, R.: The reflectance at the 950–970 nm
527 region as an indicator of plant water status, *Int. J. Remote Sens.*, 14, 1887–1905,
528 doi:10.1080/01431169308954010, 1993.

529 Porporato, A., Daly, E., and Rodriguez-Iturbe, I.: Soil water balance and ecosystem response to
530 climate change, *The American Naturalist*, 164, 625-623, 2004.

531 Reichle, R. H.: Data assimilation methods in the Earth sciences, *Adv. Water Resour.*, 31(11),
532 1411-1418, 2008.

533 Rutter, A. J., and Sands, K. (1958). The relation of leaf water deficit to soil moisture tension in
534 *Pinus sylvestris*, L. 1. The effect of soil moisture on diurnal change in water balance. *New*
535 *Phytol.* 57: 50--65.

536 Schaefli, B., & Gupta, H. V. Do Nash values have value?. *Hydrological Processes*,
537 21(15), 2075-2080, 2007.

538 Shi, J., Wang, J., Hsu, A. Y., O'Neill, P. E., and Engman, E. T.: Estimation of bare surface soil
539 moisture and surface roughness parameter using L-band SAR image data, *Geoscience and Remote*
540 *Sensing, IEEE Transactions on*, 35(5), 1254-1266, 1997.

541 Shukla, J., & Mintz, Y. (1982). Influence of land-surface evapotranspiration on the earth's climate.
542 *Science*, 215(4539), 1498-1501.

543 Sriwongsitanon, N.: Flood forecasting system development for the Upper Ping River Basin.
544 *Kasetsart Journal (Natural Science)*, 44(4), 2010.

545 Sriwongsitanon, N. and Taesombat, W.: Effects of land cover on runoff coefficient, *J. Hydrol.*,
546 410, 226–238, doi:10.1016/j.jhydrol.2011.09.021, 2011.

547 Steele-Dunne, S. C., Friesen, J., and van de Giesen, N.: Using Diurnal Variation in Backscatter to
548 Detect Vegetation Water Stress, *IEEE Transactions on Geoscience and Remote Sensing*, vol. 50,
549 issue 7, pp. 2618-2629, 2012.

550 Tucker, C. J.: Remote sensing of leaf water content in the near infrared, *Remote Sens. Environ.*,
551 10, 23–32, doi:10.1016/0034-4257(80)90096-6, 1980.

552 Ustin, S. L., Roberts, D. A., Gamon, J. A., Asner, G. P. and Green, R. O.: Using Imaging
553 Spectroscopy to Study Ecosystem Processes and Properties. *BioScience*, 54, 523–534,
554 doi:10.1641/0006-3568(2004)054[0523:UISTSE]2.0.CO;2, 2004.

555 Van Emmerik, T., Steele-Dunne, S.C., Judge, J. and van de Giesen, N.C.: Impact of Diurnal
556 Variation in Vegetation Water Content on Radar Backscatter From Maize During Water Stress,
557 *IEEE Transactions on Geoscience and Remote Sensing*, vol. 53, issue 7,
558 doi:10.1109/TGRS.2014.2386142, 2015.

559 Vermote, E. F., Kotchenova, S. Y., and Ray, J. P.: MODIS Surface Reflectance User's Guide.
560 Web site: <http://modis-sr.ltdri.org>, 2011.

561 Vrugt, J. A., Gupta, H. V., Bastidas, L. A., Bouten, W. and Sorooshian, S.: Effective and efficient
562 algorithm for multiobjective optimization of hydrologic models, *Water Resour. Res.*, 39, 1214.
563 doi:10.1029/2002WR001746, 2003.

564 Western, A. W., and Blöschl, G.: On the spatial scaling of soil moisture, *J. Hydrol.*, 217(3–4), 203-
565 224, 1999.

566 Yilmaz, M. T., Hunt, E. R. Jr., and Jackson, T. J.: Remote sensing of vegetation water content
567 from equivalent water thickness using satellite imagery, *Remote Sens. Environ.*, 112, 2514–2522,
568 [doi:10.1016/j.rse.2007.11.014](https://doi.org/10.1016/j.rse.2007.11.014), 2008.

569 Zhao, R. J.: The Xinanjiang model applied in China, *J. Hydrol.*, 135, 371–381, doi:10.1016/0022-
570 1694(92)90096-E, 1992.
571

572 Table 1. Water balance and constitutive equations used in FLEX^L.

Reservoirs	Water balance equations	Equation	Constitutive equations	Equation
Interception	$\frac{dS_i}{dt} = P - E_i - P_e$	(2)	$E_i = \begin{cases} E_0; S_i > 0 \\ 0; S_i = 0 \end{cases}$	(3)
			$P_e = \begin{cases} 0; S_i < S_{i,max} \\ P; S_i = S_{i,max} \end{cases}$	(4)
Unsaturated reservoir	$\frac{dS_u}{dt} = P_e - R - E_t$	(5)	$\frac{R}{P_e} = 1 - \left(1 - \frac{S_u}{(1 + \beta)S_{u,max}}\right)^\beta$	(6)
			$E_t = (E_0 - E_i) \cdot \min\left(1, \frac{S_u}{C_e S_{u,max} (1 + \beta)}\right)$	(7)
Splitter and Lag function			$R_f = R \cdot D$	(8)
			$R_s = R \cdot (1 - D)$	(9)
			$R_{fl}(t) = \sum_{i=1}^{T_{lag}} c(i) \cdot R_f(t - i + 1)$	(10)
			$c(i) = i / \sum_{u=1}^{T_{lag}} u$	(11)
			$Q_{fr} = \max(0, S_f - S_{f,max}) / K_{fr}$	(13)
Fast reservoir	$\frac{dS_f}{dt} = R_{fl} - Q_{ff} - Q_f$	(12)	$Q_f = S_f / K_f$	(14)
Slow reservoir	$\frac{dS_s}{dt} = R_s - Q_s$	(15)	$Q_s = S_s / K_s$	(16)

573

574 Table 2. Parameter range of the FLEX^L Model.

Parameter	Range	Parameters	Range
$S_{i,max}$ (mm)	(0.1, 6)	K_{ff} (d)	(1, 9)
$S_{u,max}$ (mm)	(10, 1000)	T_{lagF} (d)	(0, 5)
β (-)	(0, 2)	T_{lagS} (d)	(0, 5)
C_e (-)	(0.1, 0.9)	K_f (d)	(1, 40)
D (-)	(0, 1)	K_s (d)	(10, 500)
$S_{f,max}$ (mm)	(10, 200)		

575

576 Table 3. Catchment characteristics and data period for selected 8 sub-basins in the UPRB.

Sub-basin	Mae Taeng at Ban Mae Taeng (P.4A)	Nam Mae Chaem at Kaeng Ob Luang (P.14)	Ping River at Chiang Dao (P.20)	Nam Mae Rim at Ban Rim Tai (P.21)	Nam Mae Klang at Pracha Uthit Bridge (P.24A)	Nam Mae Khan at Ban Klang (P.71)	Nam Mae Li at Ban Mae E Hai (P.76)	Nam Mae Tha at Ban Sop Mae Sapuad (P.77)
Area (km ²)	1902	3853	1355	515	460	1771	1541	547
Altitude range (m)	1020	991	790	731	888	828	618	641
Average channel slope (%)	0.78	0.81	0.80	0.72	0.98	0.69	0.41	0.63
Average forest and agricultural areas (%)	81.9, 16.5	91.8, 7.4	80.9, 12.8	86.1, 11.6	79.7, 14.2	86.1, 10.1	69.7, 20.1	80.4, 12.7
Average rainfall depth (wet season/ dry season) (mm)	953 (88%) 130 (12%)	883 (92%) 75 (8%)	1076 (88%) 150 (12%)	1019 (90%) 115 (10%)	860 (88%) 121(12%)	1090 (89%) 132 (11%)	1092 (91%) 106 (9%)	757 (88%) 88 (10%)
Number of years data is coincident with NDII	11	7	12	11	12	9	12	12
Data period	1995-2011	1995-2007	1995-2012	1995-2011	1995-2012	1996-2009	1996-2012	1996-2012

577

578 Table 4. Average NDII values during the wet season, the dry season, and the whole year from
 579 2001 to 2013, and their order of moisture content (Range from 1 to 13. Less value indicates less
 580 NDII) for the entire Upper Ping River Basin.

Year	Wet season	Dry season	Annual
	(May-October)	(November-April)	
2001-2002	0.223 (2)	0.119 (7)	0.171 (4)
2002-2003	0.205 (9)	0.149 (1)	0.177 (1)
2003-2004	0.218 (5)	0.091 (12)	0.155 (12)
2004-2005	0.210 (8)	0.088 (13)	0.149 (13)
2005-2006	0.200 (11)	0.128 (3)	0.164 (7)
2006-2007	0.224 (1)	0.111 (10)	0.168 (5)
2007-2008	0.222 (3)	0.130 (2)	0.176 (2)
2008-2009	0.221 (4)	0.123 (5)	0.172 (3)
2009-2010	0.213 (7)	0.101 (11)	0.157 (11)
2010-2011	0.197 (13)	0.128 (4)	0.163 (8)
2011-2012	0.216 (6)	0.116 (9)	0.166 (6)
2012-2013	0.201 (10)	0.118 (8)	0.159 (10)
2013-2014	0.199 (12)	0.123 (6)	0.161 (9)
Average	0.211	0.118	0.165
Maximum	0.224	0.149	0.177
Minimum	0.197	0.088	0.149

581

582 Table 5. Monthly average NDII values between 2001 and 2013 and the order of basin moisture content for each of 14 sub-basins within the UPRB.

Sub-basin	Jan	Feb	Mar	Apr	May	Jun	Jul	Aug	Sep	Oct	Nov	Dec	Average
Ping River Section 1	0.14 (7.5)	0.06 (7.4)	0.02 (8.8)	0.07 (8.9)	0.17 (8.4)	0.21 (6.2)	0.22 (4.5)	0.22 (6.1)	0.24 (7.5)	0.23 (8.3)	0.22 (7.8)	0.18 (7.2)	0.16 (8)
Nam Mae Ngad	0.17 (5.2)	0.11 (5.9)	0.07 (6.2)	0.10 (6.3)	0.18 (6.9)	0.21 (7.1)	0.21 (7.5)	0.22 (8.0)	0.23 (9.2)	0.23 (7.9)	0.23 (6.4)	0.20 (5.7)	0.18 (6)
Nam Mae Taeng	0.21 (1.3)	0.16 (1.0)	0.13 (1.2)	0.14 (2.1)	0.19 (3.9)	0.21 (6.1)	0.22 (6.0)	0.23 (4.5)	0.25 (3.1)	0.25 (2.6)	0.26 (1.2)	0.24 (1.7)	0.21 (1)
Ping River Section 2	0.07 (11.5)	0.02 (9.8)	0.01 (9.2)	0.04 (11.6)	0.13 (13.1)	0.18 (13.0)	0.18 (13.5)	0.19 (13.3)	0.21 (13.6)	0.21 (12.7)	0.17 (13.4)	0.12 (13.5)	0.13 (12)
Nam Mae Rim	0.17 (5.3)	0.13 (4.3)	0.10 (3.9)	0.13 (3.3)	0.20 (2.6)	0.22 (3.7)	0.22 (4.0)	0.24 (2.5)	0.26 (1.3)	0.26 (1.2)	0.24 (3.7)	0.20 (5.6)	0.20 (2)
Nam Mae Kuang	0.09 (9.4)	0.03 (9.5)	0.02 (9.3)	0.05 (10.1)	0.15 (10.0)	0.20 (8.1)	0.21 (8.1)	0.22 (8.2)	0.24 (7.0)	0.23 (7.5)	0.20 (10.4)	0.14 (10.7)	0.15 (9)
Nam Mae Ngan	0.18 (4.0)	0.13 (4.4)	0.10 (4.9)	0.13 (4.1)	0.19 (3.9)	0.21 (5.3)	0.22 (5.5)	0.23 (5.2)	0.25 (3.9)	0.24 (4.5)	0.24 (4.5)	0.22 (4.0)	0.19 (5)
Nam Mae Li	0.05 (12.5)	-0.04 (12.5)	-0.04 (12.7)	0.02 (12.1)	0.14 (11.9)	0.19 (11.8)	0.20 (9.7)	0.23 (8.3)	0.23 (9.9)	0.21 (13.0)	0.18 (13.2)	0.13 (12.5)	0.12 (13)
Nam Mae Klang	0.19 (3.3)	0.13 (3.5)	0.12 (2.8)	0.14 (2.3)	0.20 (2.9)	0.22 (4.8)	0.22 (7.2)	0.23 (7.6)	0.23 (8.6)	0.24 (7.2)	0.24 (4.5)	0.22 (3.3)	0.20 (4)
Ping River Section 3	0.06 (11.7)	-0.03 (12.5)	-0.04 (12.3)	0.03 (11.2)	0.15 (9.3)	0.21 (7.2)	0.21 (8.7)	0.21 (9.9)	0.22 (11.4)	0.21 (11.9)	0.19 (11.2)	0.15 (10.3)	0.13 (11)
Upper Nam Mae Chaem	0.20 (1.9)	0.15 (2.0)	0.12 (2.3)	0.13 (4.2)	0.18 (6.7)	0.20 (9.5)	0.21 (9.2)	0.21 (9.1)	0.24 (6.2)	0.25 (3.9)	0.26 (2.1)	0.24 (1.6)	0.20 (3)
Lower Nam Mae Chaem	0.09 (9.8)	0.006 (10.7)	-0.007 (10.8)	0.05 (10.2)	0.15 (10.2)	0.20 (10.2)	0.20 (9.9)	0.21 (8.9)	0.23 (9.5)	0.23 (8.3)	0.21 (8.9)	0.16 (9.2)	0.14 (10)
Nam Mae Haad	0.03 (14.0)	-0.07 (14.0)	-0.06 (13.8)	0.003 (12.9)	0.15 (10.0)	0.21 (5.8)	0.22 (6.4)	0.23 (6.2)	0.24 (5.2)	0.22 (9.7)	0.19 (11.2)	0.12 (12.4)	0.12 (14)
Nam Mae Tuen	0.13 (7.6)	0.05 (7.7)	0.05 (7.0)	0.10 (5.9)	0.19 (5.2)	0.21 (6.2)	0.22 (4.9)	0.222 (7.2)	0.23 (8.7)	0.24 (6.2)	0.23 (6.5)	0.20 (6.5)	0.17 (7)
Average	0.13	0.06	0.04	0.08	0.17	0.20	0.21	0.22	0.24	0.23	0.22	0.18	0.16
Maximum	0.21	0.16	0.13	0.14	0.20	0.22	0.22	0.24	0.26	0.26	0.26	0.24	0.21
Minimum	0.03	-0.07	-0.06	0.003	0.13	0.18	0.18	0.19	0.21	0.21	0.17	0.12	0.12

583

584

585 Table 6. FLEX^L parameters calibrated at 8 runoff stations located in the UPRB.

Runoff station	S _{i,max} (mm)	S _{u,max} (mm)	Ce (-)	Beta (-)	D (-)	K _f (days)	K _s (days)	T _{lagF} (days)	T _{lagS} (days)	S _{f,max} (mm)	K _{ff} (days)
P.4A	2.0	463	0.30	0.66	0.77	2.9	42	1.1	49	93	9.1
P.14	2.3	269	0.55	1.16	0.65	4.0	63	1.5	39	155	7.6
P.21	2.3	388	0.31	0.90	0.64	2.1	66	2.4	48	33	2.5
P.20	2.0	324	0.47	0.50	0.79	7.7	103	1.0	25	69	1.7
P.24A	3.2	209	0.77	1.53	0.89	3.2	267	1.5	44	24	4.2
P.76	2.3	486	0.62	0.32	0.89	2.4	191	2.7	3	130	7.4
P.77	4.5	344	0.48	0.27	0.75	1.5	65	1.2	30	164	5.6
P.71	4.3	532	0.34	0.46	0.90	3.5	80	1.8	15	179	6.5

586

587 Table 7. FLEX^L model performance at 8 runoff stations.

Station	Data period	I_{KGE}	I_{KGL}	I_{KGF}
P.4A	1995-2009	0.822	0.667	0.963
P.14	1995-2007	0.796	0.442	0.966
P.21	1995-2009	0.814	0.718	0.985
P.20	1995-2011	0.792	0.685	0.964
P.24A	1995-2011	0.623	0.598	0.945
P76	2000-2011	0.539	0.665	0.916
P.77	1999-2011	0.775	0.612	0.970
P.71	1996-2009	0.823	0.714	0.975
Average		0.748	0.638	0.961

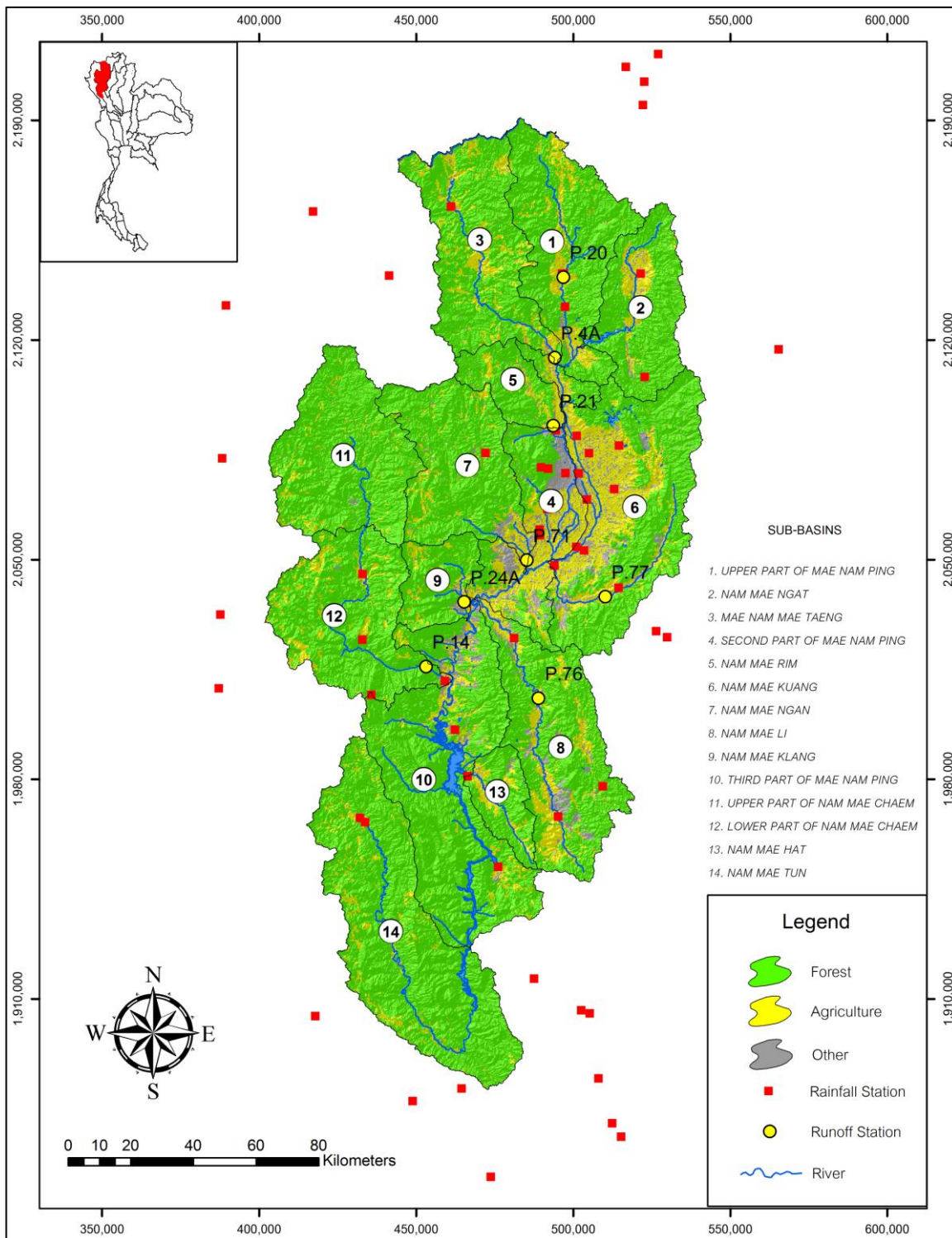
588

589 Table 8. Exponential relationships between the average NDII values and simulated root zone
 590 moisture storage (S_u) in the 8 sub-basins controlled by the 8 runoff stations.

Runoff station	Annual Relationship			Wet Season Relationship			Dry Season Relationship		
	a	b	R ²	a	b	R ²	a	b	R ²
P.4A	11.2	12.4	0.66	11.1	12.9	0.53	12.6	11.2	0.90
P.14	21.9	9.8	0.81	19.2	10.8	0.71	24.6	8.5	0.92
P.20	52.3	7.4	0.79	36.2	9.1	0.72	59.7	6.7	0.91
P.21	30.8	9.0	0.68	27.8	9.3	0.53	30.6	9.22	0.86
P.24A	22.1	8.5	0.60	24.2	8.3	0.41	22.4	8.1	0.81
P.71	2.1	19.9	0.77	1.9	20.5	0.65	2.3	19.0	0.87
P.76	10.1	13.6	0.85	8.1	14.4	0.74	10.8	14.6	0.87
P.77	35.4	8.0	0.70	20.7	10.2	0.61	40.6	7.7	0.83
Averag e	-	-	0.73	-	-	0.61	-	-	0.87

591 Note: $S_u = ae^{bNDII}$

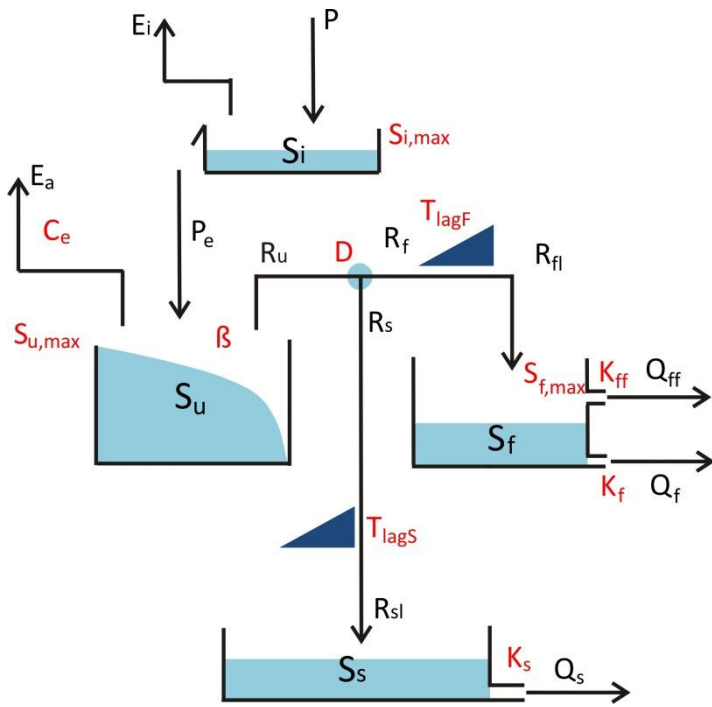
592



593

594

595 Figure 1. The Upper Ping River Basin (UPRB) and the locations of the rain-gauge and runoff
 596 stations. The numbers indicate the 14 sub-basins of the UPRB.



597
 598
 599
 600
 601

Figure 2. Model structure of the FLEX^L.

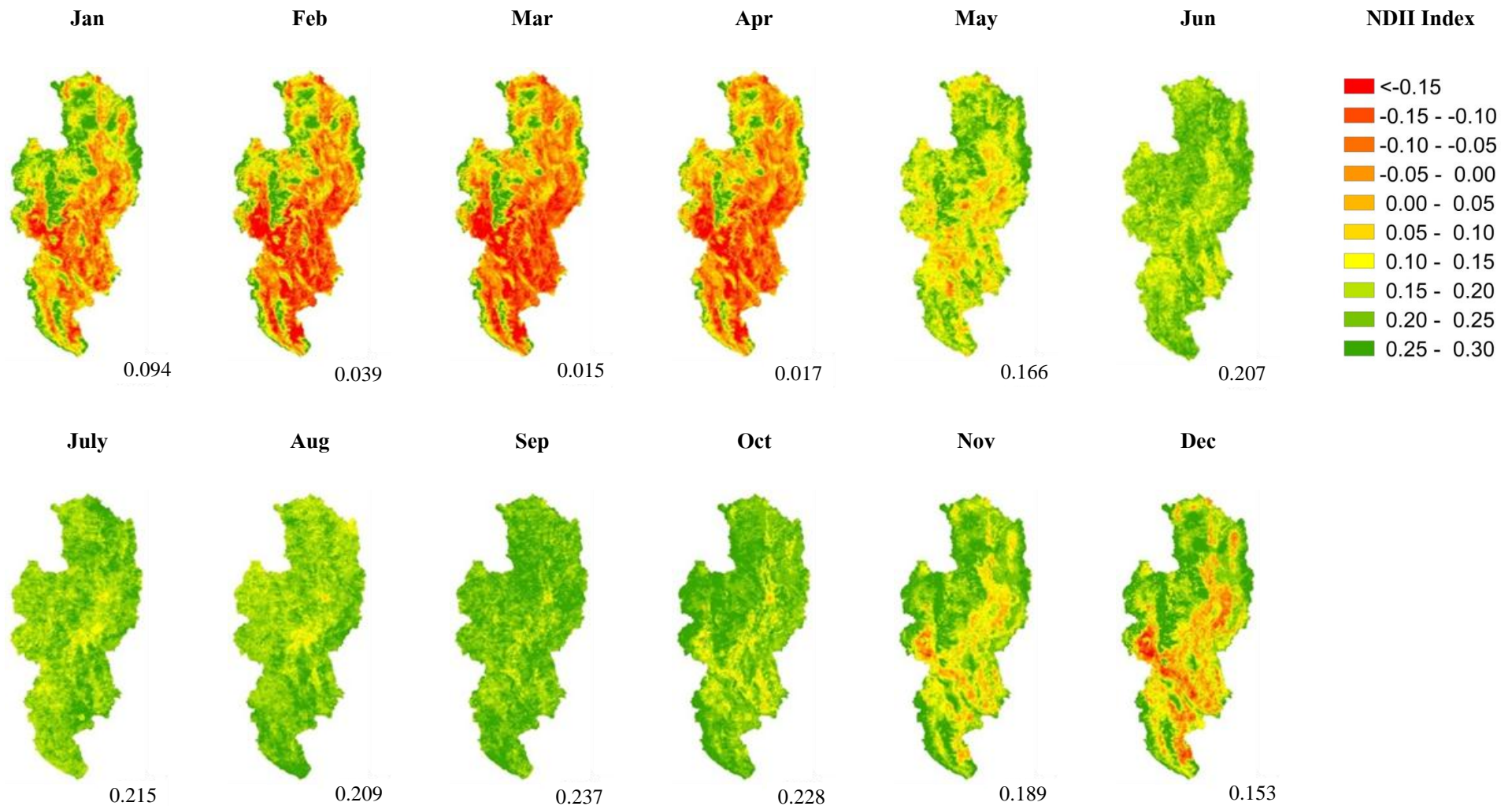


Figure 3. Monthly average NDII values for the UPRB in 2004. The green color indicates an NDII between 0.15 and 0.30, yellow between 0 and 0.15, orange between -0.15 and 0 and red an NDII<-0.15) representing relatively high-, medium-, low-, and very low- root zone moisture content.

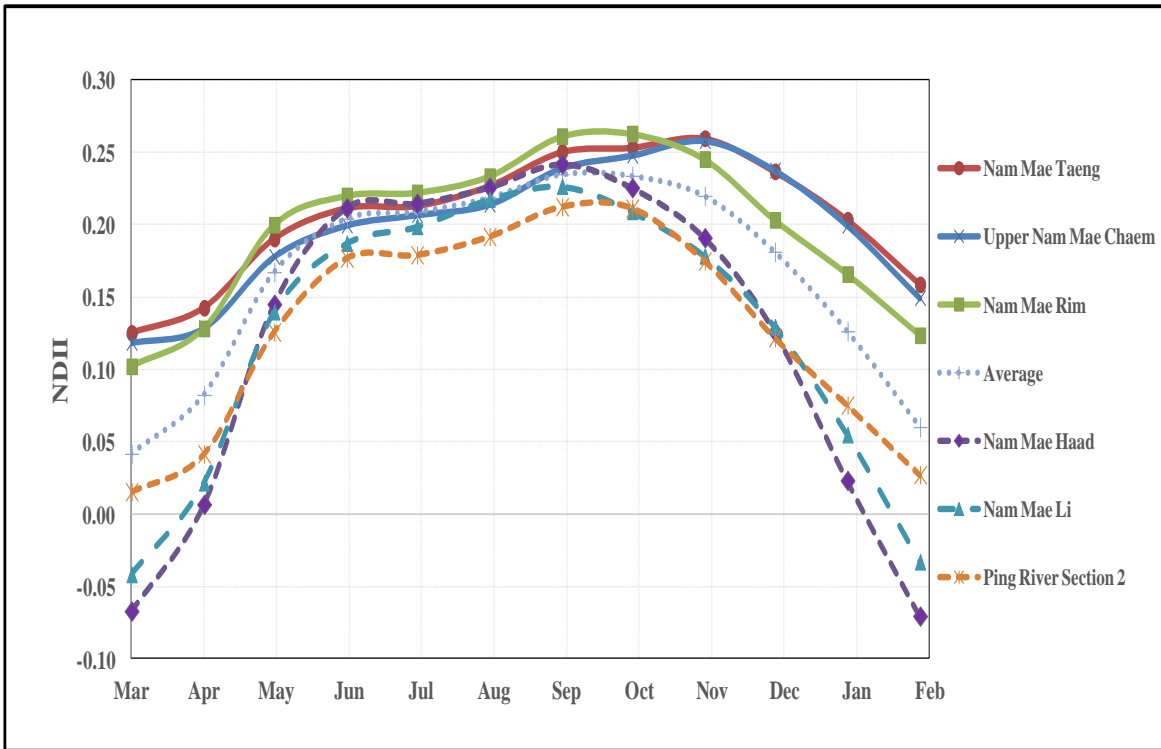


Figure 4. Monthly average NDII values for 6 sub-basins compared to the basin average in the UPRB. Note that three wettest and three driest basins are presented in this graph.

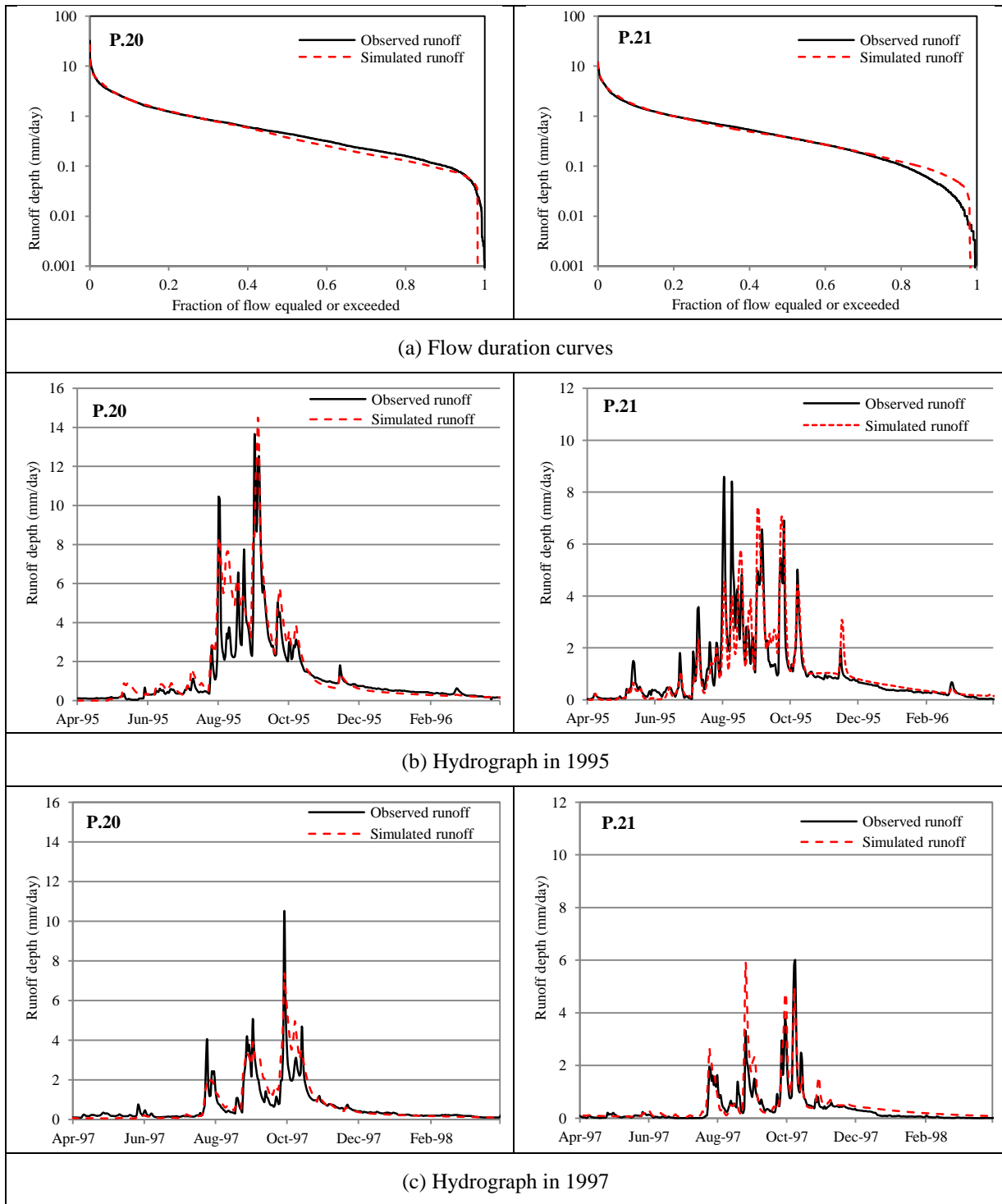


Figure 5. Examples of flow duration curves and simulated hydrographs using FLEX^L at runoff stations P.20 and P.21.

Runoff Station	Annual	Wet Season	Dry Season
P.4A	<p>8-day average S_u (mm)</p> <p>$y = 19.836e^{10.675x}$ $R^2 = 0.6105$</p> <p>8-day average NDII</p>	<p>8-day average S_u (mm)</p> <p>$y = 39.272e^{8.188x}$ $R^2 = 0.2821$</p> <p>8-day average NDII</p>	<p>8-day average S_u (mm)</p> <p>$y = 17.637e^{10.709x}$ $R^2 = 0.8329$</p> <p>8-day average NDII</p>
P.14	<p>8-day average S_u (mm)</p> <p>$y = 27.919e^{9.237x}$ $R^2 = 0.7979$</p> <p>8-day average NDII</p>	<p>8-day average S_u (mm)</p> <p>$y = 38.13e^{8.137x}$ $R^2 = 0.4418$</p> <p>8-day average NDII</p>	<p>8-day average S_u (mm)</p> <p>$y = 28.537e^{8.518x}$ $R^2 = 0.8696$</p> <p>8-day average NDII</p>
P.20	<p>8-day average S_u (mm)</p> <p>$y = 13.373e^{11.922x}$ $R^2 = 0.8605$</p> <p>8-day average NDII</p>	<p>8-day average S_u (mm)</p> <p>$y = 17.883e^{11.002x}$ $R^2 = 0.5434$</p> <p>8-day average NDII</p>	<p>8-day average S_u (mm)</p> <p>$y = 13.817e^{10.79x}$ $R^2 = 0.8727$</p> <p>8-day average NDII</p>
P.21	<p>8-day average S_u (mm)</p> <p>$y = 39.629e^{7.794x}$ $R^2 = 0.6169$</p> <p>8-day average NDII</p>	<p>8-day average S_u (mm)</p> <p>$y = 62.255e^{5.959x}$ $R^2 = 0.2339$</p> <p>8-day average NDII</p>	<p>8-day average S_u (mm)</p> <p>$y = 34.717e^{8.476x}$ $R^2 = 0.7895$</p> <p>8-day average NDII</p>

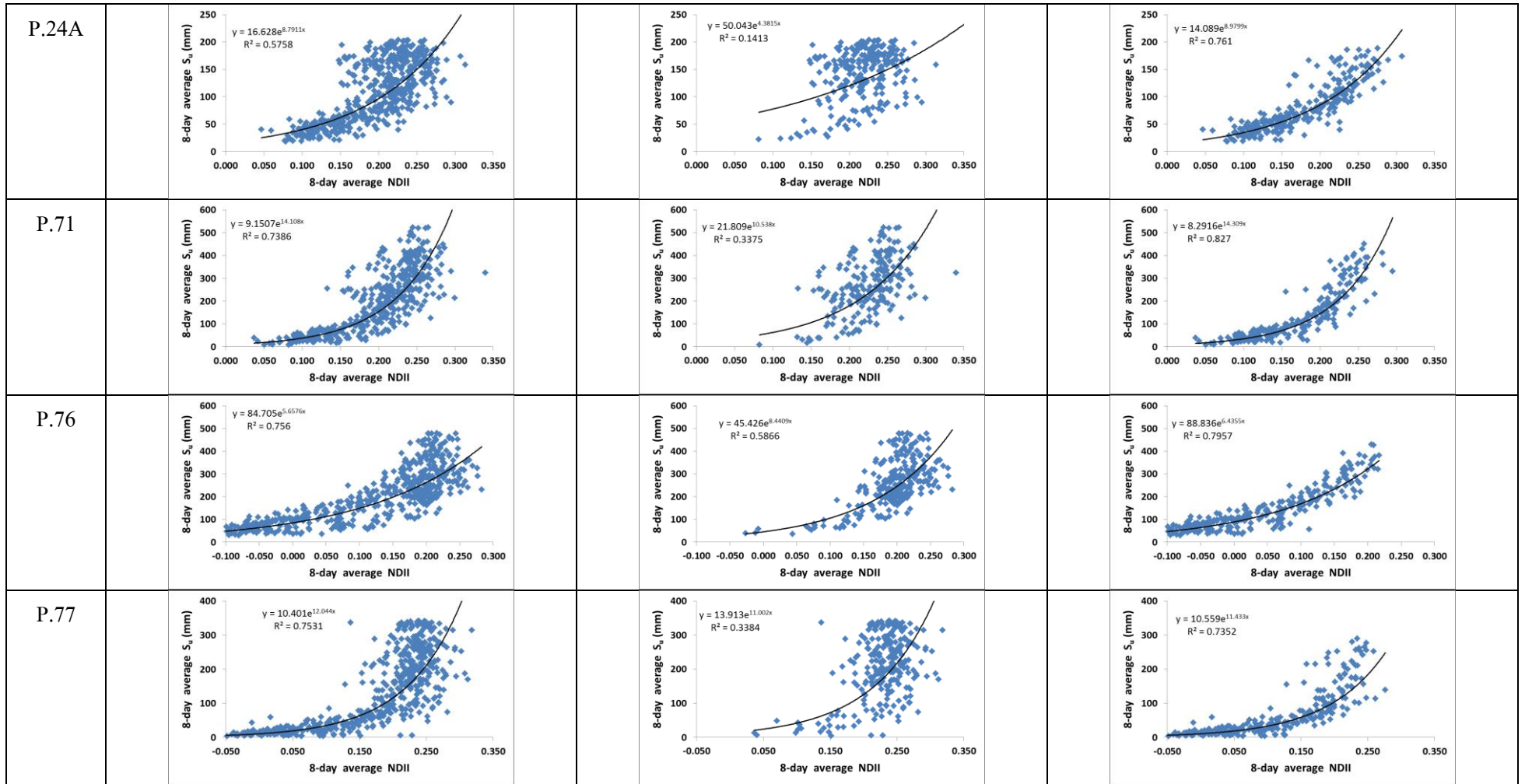


Figure 6. Scatter plots between the average NDII and the average root zone moisture storage (S_u) for 8 sub-basins controlled by runoff stations.

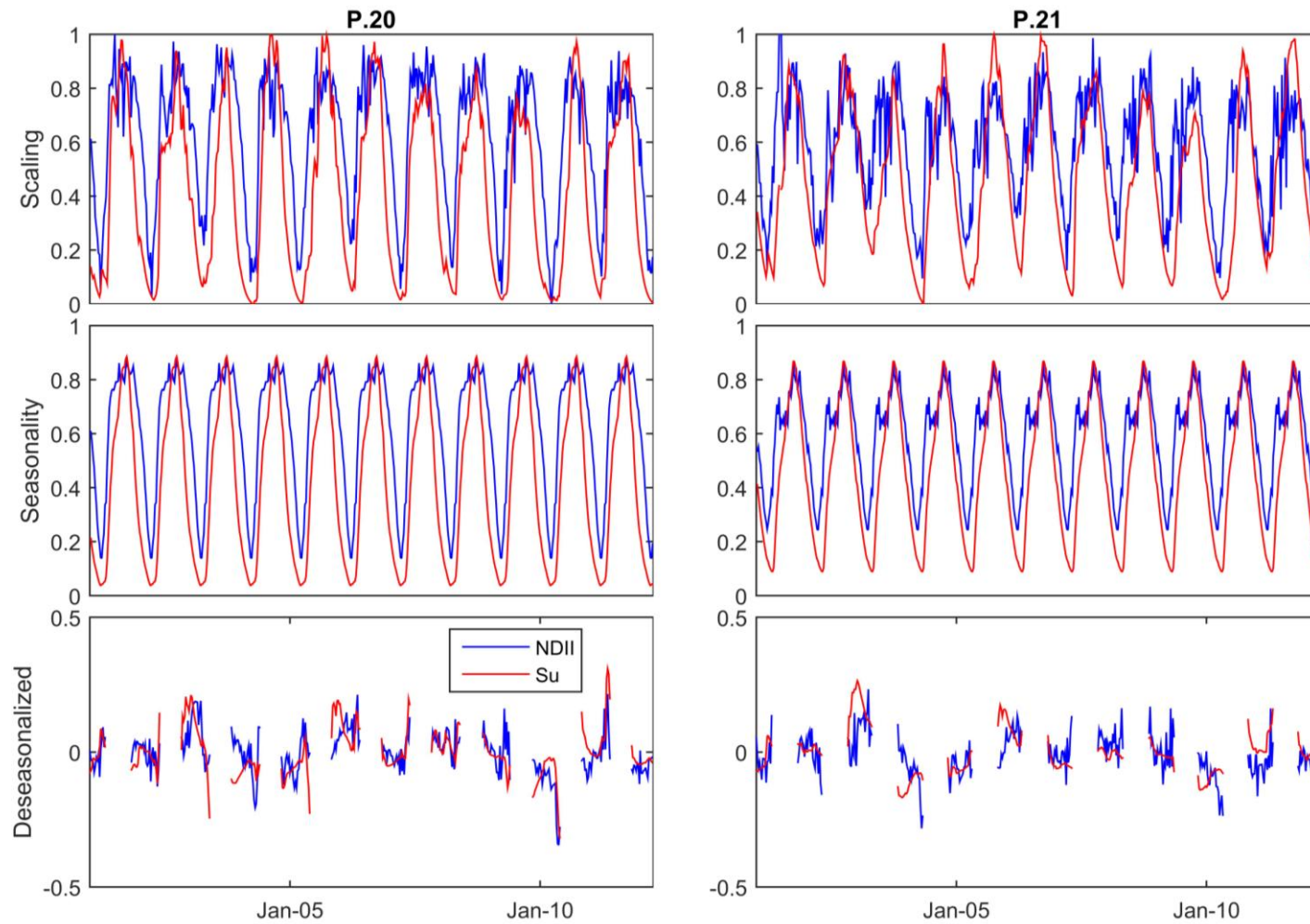


Figure 7. Scaled time series, seasonality and de-seasonalized (dry seasons) time series of the 8-days-averaged NDII values compared to the 8-days-averaged simulated root zone moisture storage (S_u) in Nam Mae Rim sub-basin at P.20 (Chiang Dao) and P.21 (Ban Rim Tai) runoff stations. The coefficients of determination (R^2) of the de-seasonalized NDII and S_u are 0.32 and 0.18 respectively for P.20 and P.21. For the results of all the 8 sub-basins, please refer to the supplementary material.